Clinical Cancer Research

HDAC Inhibitors Enhance T-Cell Chemokine Expression and Augment Response to PD-1 Immunotherapy in Lung Adenocarcinoma

Hong Zheng[1], Weipeng Zhao[1,2], Cihui Yan[1,2], Crystina C. Watson[1,3], Michael Massengill[1], Mengyu Xie[1,3], Chris Massengill[1], David R. Noyes[1], Gary V. Martinez[4], Roha Afzal[4], Zhihua Chen[5], Xiubao Ren[2], Scott J. Antonia[1,6], Eric B. Haura[6], Brian Ruffell[1,7], and Amer A. Beg[1,6]

Abstract

Purpose: A significant limitation of checkpoint blockade immunotherapy is the relatively low response rate (e.g., ~20% with PD-1 blockade in lung cancer). In this study, we tested whether strategies that increase T-cell infiltration to tumors can be efficacious in enhancing immunotherapy response.

Experimental Design: We performed an unbiased screen to identify FDA-approved oncology agents with an ability to enhance T-cell chemokine expression with the goal of identifying agents capable of augmenting immunotherapy response. Identified agents were tested in multiple lung tumor models as single agents and in combination with PD-1 blockade. Additional molecular and cellular analysis of tumors was used to define underlying mechanisms.

Results: We found that histone deacetylase (HDAC) inhibitors (HDACi) increased expression of multiple T-cell chemokines in cancer cells, macrophages, and T cells. Using the HDACi romidepsin *in vivo*, we observed increased chemokine expression, enhanced T-cell infiltration, and T-cell–dependent tumor regression. Importantly, romidepsin significantly enhanced the response to PD-1 blockade immunotherapy in multiple lung tumor models, including nearly complete rejection in two models. Combined romidepsin and PD-1 blockade also significantly enhanced activation of tumor-infiltrating T cells.

Conclusions: These results provide evidence for a novel role of HDACs in modulating T-cell chemokine expression in multiple cell types. In addition, our findings indicate that pharmacologic induction of T-cell chemokine expression represents a conceptually novel approach for enhancing immunotherapy response. Finally, these results suggest that combination of HDAC inhibitors with PD-1 blockade represents a promising strategy for lung cancer treatment. *Clin Cancer Res; 22(16); 4119–32. ©2016 AACR.*

Introduction

Lung cancer is a leading cause of cancer-related death around the world, and the 5-year survival has remained unchanged for decades. Importantly, recent studies have demonstrated the considerable potential of immunotherapy in the treatment of lung cancer and other malignancies (1, 2). In particular, blockade of CTLA-4 and PD-1 checkpoint cell surface receptors on T cells is a promising approach (3, 4). CTLA-4 and PD-1 deliver inhibitory signals following binding to their ligands CD80/86 and PD-L1/2, respectively, and blocking binding of these ligands with antibodies augments antitumor T-cell responses (1, 2). PD-1 blockade is an especially promising approach (3, 4), yet response rates are relatively low at approximately 20% in lung cancer, indicating that combinatorial approaches are needed to enhance efficacy. Combinatory therapies currently being evaluated include blockade of multiple checkpoint receptors, as well as use of vaccines, radiation, and agonistic mAb (1, 5, 6). There is growing interest in efficacious combinations of small-molecule chemotherapeutics with immunotherapy to enhance response rates (6–8). Several traditional therapies are dependent upon immune activation, including induction of immunogenic cell death (e.g., by anthracyclines; ref. 9), an increase in granzyme B permeability of tumor cells (e.g., by taxol; ref. 10), and alterations in metabolite and amino acid levels within the tumor microenvironment (7, 11). In this study, we tested the hypothesis that strategies which increase expression of T-cell chemokines and T-cell infiltration to tumors will be especially efficacious in enhancing response to PD-1 blockade.

Previous studies have demonstrated that increased tumor expression of T-cell chemokines, such as *CCL5* and *CXCL10*, is associated with a better response to immunotherapy (12).

[1]Department of Immunology, Moffitt Cancer Center, Tampa, Florida. [2]Tianjin Medical University Cancer Institute and Hospital, National Clinical Research Center for Cancer, Key Laboratory of Cancer Prevention and Therapy, Tianjin, China. [3]Department of Cancer Biology PhD Program, University of South Florida, Tampa, Florida. [4]Department of Cancer Imaging and Metabolism, Moffitt Cancer Center, Tampa, Florida. [5]Department of Bioinformatics, Moffitt Cancer Center, Tampa, Florida. [6]Department of Thoracic Oncology, Moffitt Cancer Center, Tampa, Florida. [7]Department of Breast Oncology, Moffitt Cancer Center, Tampa, Florida.

Note: Supplementary data for this article are available at Clinical Cancer Research Online (http://clincancerres.aacrjournals.org/).

H. Zheng and W. Zhao contributed equally to this article.

Corresponding Author: Amer A. Beg, H. Lee Moffitt Cancer Center & Research Institute, 12902 Magnolia Dr, Tampa, FL 33612. Phone: 813-745-5714; Fax: 813-745-7265; E-mail: amer.beg@moffitt.org

doi: 10.1158/1078-0432.CCR-15-2584

Translational Relevance

Insufficient tumor-infiltrating T cells are recognized as a major resistance mechanism to immunotherapy. Here, we tested the hypothesis that strategies which increase the expression of T-cell chemokines and T-cell infiltration to tumors will be efficacious in enhancing immunotherapy response. We utilized a screening approach to identify FDA-approved oncology agents and discovered a novel ability of HDAC inhibitors (HDACi) to induce the expression of T-cell chemokines. HDAC inhibitors strongly augmented response to PD-1 immunotherapy in multiple lung tumor models. Our findings indicate that approaches utilizing induction of T-cell chemokine expression represent a conceptually novel strategy for enhancing immunotherapy response. The combination of HDACi and PD-1 blockade will be tested in several clinical trials, including a trial in NSCLC at our institution. We believe the findings described in this study can provide a framework for mechanistic assessment of the impact of this combination on patient tumors.

Furthermore, expression of T-cell chemokines is strongly and positively associated with increased T-cell infiltration and improved patient survival (13–15). Conversely, poor T-cell infiltration in tumors can be associated with resistance to immunotherapy. On the basis of these findings, we tested the hypothesis that oncology agents capable of enhancing expression of T-cell–attracting chemokines will augment the response to immunotherapy. To this end, we screened a library of FDA-approved oncology agents specifically for their ability to induce expression of T-cell chemokines. Interestingly, only a single class of agents, histone deacetylase (HDAC) inhibitors (HDACi), were found to robustly induce expression of multiple chemokines in tumor cells, tumor-infiltrating macrophages, and T cells. HDACi romidepsin treatment triggered a strong antitumor immune response in mice and enhanced PD-1 blockade immunotherapy in multiple tumor models. These findings indicate the significant potential benefit of pairing checkpoint blockade immunotherapy with HDACi for near-term clinical use. In addition, our findings indicate that therapeutic approaches which upregulate T-cell chemokine expression represent a novel strategy for augmenting the response to immunotherapy.

Materials and Methods

Mice, cells, and reagents

All mice were bred and housed in the animal facility at Moffitt Cancer Center under specific pathogen-free conditions. 129S4/SvJaeJ mice were obtained from Jackson Laboratories. All animal experiments were performed in accordance with the Institutional Animal Care and Use Committee. Mouse LKR-13 had KRAS G12D mutation (16) while 393P and 344SQ (kindly provided by Dr. J. Kurie, MD Anderson Cancer Center, Houston, TX) had KRAS G12D and TP53 mutations (R172H; ref. 17). For bioluminescence imaging, LKR cells were transduced with a replication-deficient lentivirus in which luciferase expression was driven by the thymidine kinase promoter. All lung cancer cell lines were maintained in RPMI1640 with 10% FBS. $CD11b^+$ cells were isolated from LKR tumors using microbeads (Miltenyi Biotec) and cultured in DMEM media. Forty-eight hours later, nonadherent cells were removed and attached cells were stimulated with romidepsin. FDA-approved oncology agents were utilized from the Approved Oncology Drugs Set (97 agents) provided by the Developmental Therapeutics Program of NCI (Bethesda, MD). Anti-mCD4 (Clone GK1.5), mCD8 (Clone 2.43), mIFNγ (Clone R4-6A2), and mPD-1 (Clone RMP1-14) were purchased from Bio-X-Cell, along with matching isotype controls. Romidepsin and other HDACi were purchased from Selleckchem and used at the following concentrations: vortinostat 10 μmol/L, MS275 0.5 μmol/L, MGCD0103 1 μmol/L, and LBH-589 0.1 μmol/L. mIFNγ (25 ng/mL) was purchased from eBioscience and hIFNγ (100 ng/mL) from Pestka Biomedical. TAK-779 was purchased from Sigma and Collagenase D was from Roche.

High-throughput viability assay and screening

FDA-approved oncology agents were utilized from the Approved Oncology Drugs Set (97 agents) from the Developmental Therapeutics Program of NCI. Beckman-Coulter Biomek FX^P robotic liquid handling system was used for drug treatment in 96-well plates following which cell viability was determined. Briefly, LKR cells were plated in 96-well plates at a concentration of 2,000 cells/100 μL of RPMI with 10% FBS. Twenty-four hours later, oncology agents were individually introduced in triplicate wells in DMSO to achieve final concentrations of 10 μmol/L, 1 μmol/L, 0.1 μmol/L, and 0.01 μmol/L. A viability assay was performed 48 hours after drug administration using Cell Counting Kit-8 (Dojindo Laboratories) as per the manufacturer's instructions. Absorbance for the standard curve was determined 24 hours after plating 2,000, 1,000, 500, 250, 125, and 62.5 LKR cells per 100 μL. Lethal dose 50 (LD_{50}) values for oncology agents were calculated using "Dose–response – Inhibition: log(inhibitor) versus normalized response" in GraphPad Prism 5 software. Agents which did not induce cell death were used at 10 μmol/L (see Supplementary Table S1). LD_{50} of romidepsin for LKR at 48 hours was 23 nmol/L. However, the LD_{50} range in different lung cancer lines used here was 23–35 nmol/L. To treat different cell lines with the same romidepsin concentration, we used it at 30 nmol/L.

RNA analysis, microarray studies, ELISA

RNA was isolated using a Qiagen RNeasy Kit, reverse transcribed, and subjected to quantitative PCR analysis, as described previously (13, 18). For tumor RNA analysis, tumors were frozen in liquid nitrogen and homogenized in a Bead Beater. Tumor RNA was extracted using Qiagen RNeasy Kit. Microarray analysis was performed using the Mouse Genome 430 2.0 Arrays as described previously (13).

Tumor studies

Cells were harvested in logarithmic growth phase after being cultured for less than 2 weeks, washed once in injection medium (phenol-free DMEM supplemented with 2% FBS), and counted. A total of 1×10^6 cells were injected subcutaneously and tumors were monitored for growth by measurements 2–3 times per week. The tumor volume was determined as length × length × width/2. Romidepsin was injected intraperitoneally (2 mg/kg) on days 14, 16, and 18 after tumor inoculation. Anti-PD-1 was injected intraperitoneally (300 μg/mouse per injection) on days 15, 17,

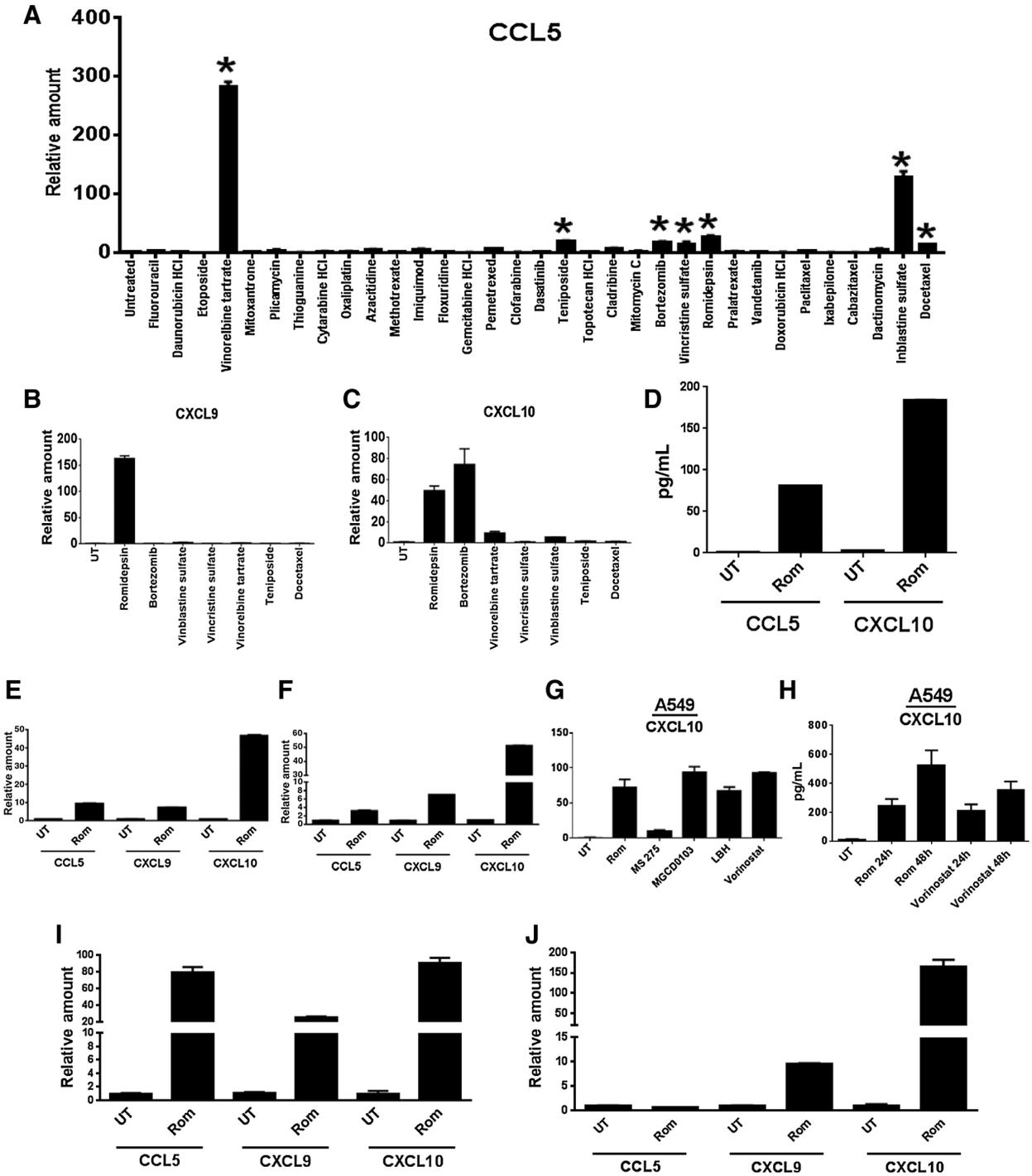

Figure 1.

HDACi induce expression of multiple T-cell chemokines in mouse and human lung cancer cell lines. **A,** *Ccl5* mRNA expression was determined by real-time PCR in LKR cells after treatment with a subset of oncology agents that induced cytotoxicity. Expression was normalized to ribosomal 18s RNA and is shown as fold change compared with DMSO-treated LKR (set at 1). Asterisks indicate 10-fold or greater increase in expression. Samples were run in triplicate and reported as mean ± SEM. *Cxcl9* (**B**) and *Cxcl10* (**C**) mRNA expression is shown following 24-hour treatment of LKR cells with indicated agents. Expression levels were determined as in Fig. 1A. **D,** secreted levels of CCL5 and CXCL10 in LKR cells were determined by ELISA following romidepsin treatment (30 nmol/L) for 48 hours. **E** and **F,** *Ccl5, Cxcl9*, and *Cxcl10* mRNA expression in mouse lung cancer line 344SQ and human lung cancer line A549 was determined 24 hours after treatment with romidepsin (30 nmol/L). **G,** *CXCL10* mRNA expression was determined in A549 following treatment with 30 nmol/L romidepsin, 500 nmol/L MS275, 1 μmol/L MGCD0103, 100 nmol/L LBH-589, and 10 μmol/L vorinostat for 24 hours. **H,** secreted levels of *Cxcl10* in A549 were determined by ELISA following 30 nmol/L romidepsin or 10 μmol/L vorinostat treatment for indicated time periods. **I,** mouse raw macrophages were treated with romidepsin (30 nmol/L) following which mRNA expression of *Ccl5, Cxcl9*, and *Cxcl10* was determined. **J,** $CD11b^{+}$ cells were isolated from LKR tumors and cultured for 2 days following which adherent macrophages were stimulated with romidepsin (30 nmol/L) for 24 hours and mRNA expression of *Ccl5, Cxcl9*, and *Cxcl10* was determined. UT, untreated; Rom, romidepsin.

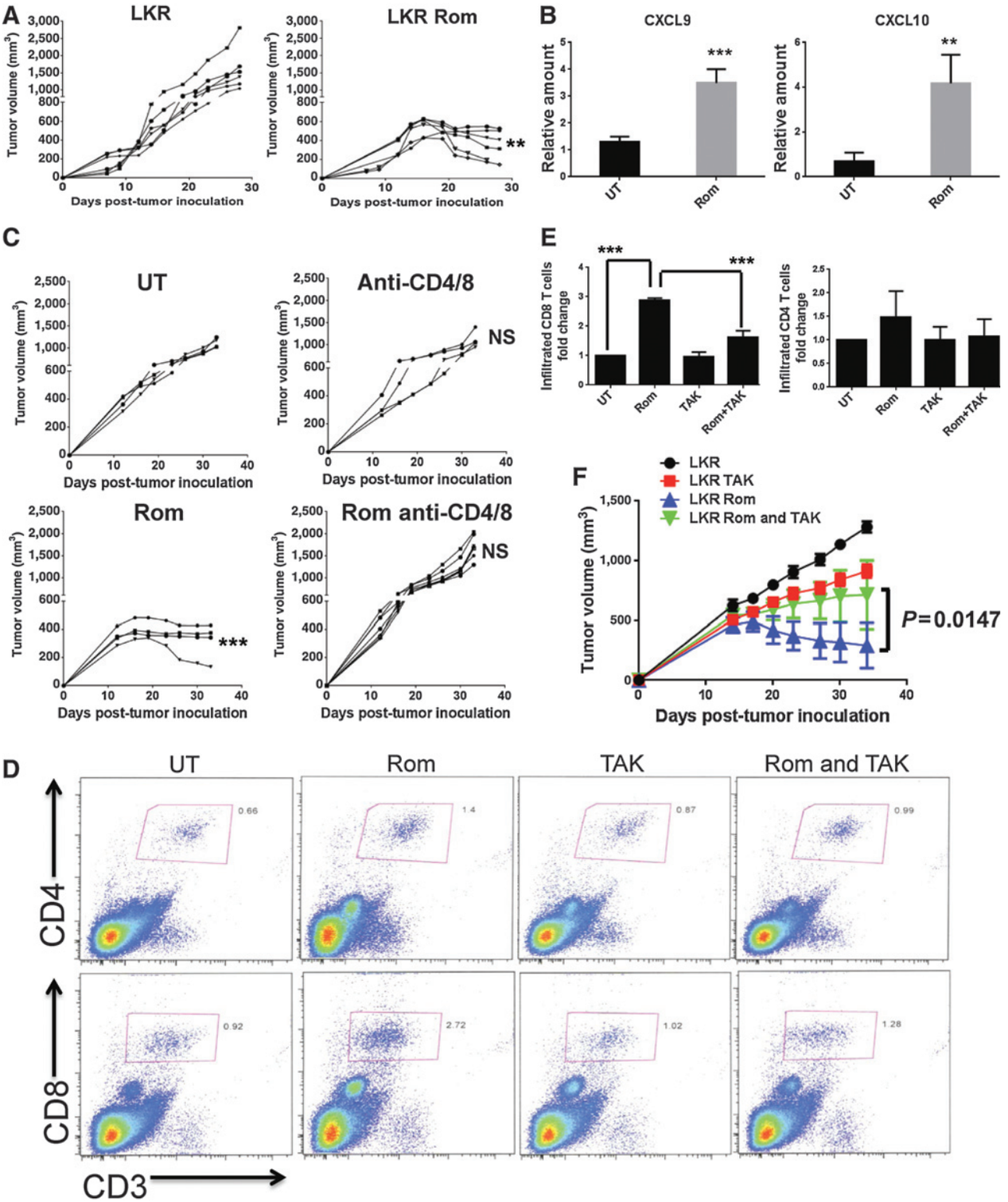

Figure 2.

Antitumor effect of romidepsin accompanies increased T-cell chemokine expression and is critically dependent on T cells. **A,** 129 mice were inoculated subcutaneously with 10^6 LKR cancer cells. Effect of romidepsin (Rom) treatment (2 mg/kg on days 14, 16, 18) on tumor growth over indicated time periods is shown. Each line represents a single mouse. Significance of tumor size difference is indicated compared with untreated control mice at the last timepoint. **B,** *Cxcl9* and *Cxcl10* mRNA expression was determined in day 16 subcutaneous LKR tumors by RT-PCR after two romidepsin injections. UT, untreated mice. Results shown represent 3–4 tumors that were individually analyzed. (*Continued on the following page.*)

and 19 after tumor inoculation. Isotype controls were injected in control mice. Anti-CD4 and anti-CD8 (300 μg/mouse) were injected intraperitoneally as indicated in Supplementary Fig. S3. TAK-779 (150 μg/mouse) or anti-IFNγ (200 μg/mouse) was injected on day 12 and then twice a week. Mice were sacrificed when subcutaneous tumors reached a diameter of 20 mm or when they showed signs of morbidity. Relative tumor size between treatment groups was analyzed using the *t* test with Welch correction. To determine presence of infiltrating T cells, tumors were chopped using forceps and scalpels, digested in the Collagenase D buffer with 2 mg/mL Collagenase D at 37°C for 45 to 75 minutes, passed through 70-μm strainer, and then subjected to FACS analysis as indicated in figures. In the orthotopic model, 50,000 tumor cells were injected percutaneously into the left lateral thorax in mice anesthetized with sodium pentobarbital (50 mg/kg body weight). For bioluminescence imaging (BLI) in the orthotopic model, the IVIS Imaging system was used as described previously (19). A conditional mutant $KRAS^{G12D}$ autochthonous knock-in mouse model of lung cancer (20) was obtained from Jackson Laboratories. At approximately 6 weeks of age, $KRAS^{G12D}$ mice were injected with 5×10^6 PFU of adenovirus-expressing CRE (Ad-CRE) through the intratracheal (i.t.) route. Pretreatment tumor volume was determined by MRI to noninvasively monitor and assess tumor volumes longitudinally starting at 3 months after Ad-CRE injection. 2 rounds of romidepsin+anti-PD-1 treatment, as described in subcutaneous model, were given immediately and 2 weeks after determining pretreatment tumor volumes. Posttreatment MRI was performed 4 weeks after pretreatment MRI. These studies were performed in the Moffitt Small Animal Imaging Laboratory (SAIL) Core facility using a 7-T horizontal magnet (ASR 310, Agilent Technologies).

MRI studies

Mice were placed in an induction chamber and anesthetized with 2% isoflurane for transfer onto a mouse cradle and maintained under anesthesia. A respiration pad was used for monitoring respiration rate, where a steady state breathing rate of 50 to 60 breaths per minute was achieved. A fiber optic rectal thermometer was used to monitor the temperature, and a core body temperature of 37 ± 1°C was sustained. The MRI experiments were done on a 7 Tesla Agilent ASR 310 equipped with nested 205/120/HDS gradient insert in a bore size of 310 mm. Two RF coils, a 35-mm Litzcage coil (Doty Scientific, Inc.) and a 24-mm Litzcage coil (Doty Scientific, Inc), were used depending on the sizes and weights of the mice. Coronal multislice T_2-weighted fast spin echo images were acquired with TE = 30.05 ms, TR = 1497.52 ms, field of view of 90 × 40 mm^2, and, 20 slices of 1.2 mm thickness and a data matrix of 256 × 128 × 20. Rather than using respiratory gating, additional images were acquired to offset the effects of motion (32 averages). These images were acquired within 13 minutes. To quantify the tumor burden within the lungs, T_2-weighted images were used to manually draw regions of interest with the Image Processing Toolbox in MATLAB. These were done on a slice-by-slice basis, and care was taken to avoid the heart, blood vessels, and the mediastinum. Tumors were segmented using Otsu multi-thresholding, and total tumor volume was determined by summing those lesions for all slices within the total multislice volume of interest. This was an iterative process, and additional T_1-weighted images, and multislice maximum intensity projections were used to discriminate vessel from lesion.

ELISPOT

ELISPOT was used to detect IFNγ produced by CD8 and CD4 T cells as described (21). Mouse tumor cells were processed as described previously (22) and subjected to the magnetic bead separation for isolating CD8 T and CD4 T cells according to manufacturer's recommendations (Miltenyi Biotec). Next, 4×10^5/well CD8 or CD4 T cells and 1×10^5/well of 5,000 rads irradiated tumor cells were plated in triplicate wells and incubated in 96-well plates at 37°C for 24 hours. LKR cells were stimulated with IFNγ to increase MHC expression. T cells were also cultured alone or with Concavalin A as negative and positive controls, respectively. Plates were washed 6 times with PBS + 0.05% Tween 20 and 100 μL/well of biotinylated anti-IFNγ detecting antibody (eBioscience, cat no. 13-7312-85) diluted to 1 μg/mL in PBS + 0.05% Tween 20 was added. Avidin-HRP (BD Biosciences, cat no. 554058) was used as detection reagent. Spot counting was done with an AID ELISPOT Reader System (Autoimmun Diagnostika GmbH).

Flow cytometric analysis

Cells were incubated for 5 minutes at room temperature with Fc block and DAPI was added prior to analysis to assess viability. Flow cytometric analysis was performed on an LSR II cytometer (BD Biosciences). Data were acquired using CellQuest software (BD Biosciences) and analyzed using FlowJo software (Tree Star). For tumor-infiltrating T cells, cells were gated on strict forward and side scatter parameters to ensure single-cell analysis. In addition, the DAPI- population was used for viable cells. Finally, cells were assessed for CD3 and CD4 or CD8 expression. The following FACS antibodies were used: APC anti-mouse MHC Class I (H-2Kb; cat no. 17-5958-82) and PE-Cyanine 7 anti-Mouse CD45 (cat no. 25-0451-82) were purchased from eBioscience, PE CD274 (B7-H1, PD-L1) anti-mouse mAb (clone MIH5; cat no. A14764) was from Life Technologies, Biotin anti-mouse CD95 (Cat No. 554256), anti-mouse CD16/CD32 (Mouse BD Fc Block; cat no. 553142) PE anti-mouse CD3 (cat no. 553063), FITC anti-mouse CD4 (cat no. 553729), and PerCP-Cy5.5 anti-mouse CD8 (cat no. 551162), were from BD Biosciences. Cell culture supernatants were tested for presence of IFNγ using a CBA assay (BD Biosciences).

(*Continued.*) **C,** same as in A except, where indicated, depleting antibodies to CD8 and CD4 T cells were injected. **D,** mice with day 14 tumors were untreated or treated with romidepsin on days 14 and 16 after which different group tumors (3–4 tumors) were pooled before FACS to determine CD4 ($CD3^+CD4^+$) and CD8 ($CD3^+CD8^+$) percentages in total viable cells (day 17). TAK-779 (TAK; 150 μg/mouse) was injected on day 12 and 15 where indicated. **E,** combined results of three independent experiments showing fold increase in presence of CD8 and CD4 T cells in tumors compared with untreated tumors (set at 1) after indicated treatments. Statistical significance (*t* test) is shown for indicated comparisons. **F,** effect of romidepsin and TAK-779 on tumor growth over indicated time periods. Romidepsin treatment was same as in A. TAK-779 was injected 2 days prior to romidepsin treatment and continued for twice a week for the length of the experiment. Measurement of five tumors/group are indicated as mean ± SEM. Statistical significance is indicated as *, $P < 0.05$; **, $P < 0.01$; ***, $P < 0.001$. NS, not significant.

Statistical analysis

Statistical analysis was performed using two-tailed Student *t* test, Student *t* test with Welch correction, and Fisher exact test. GraphPad Prism 5 software (GraphPad Software Inc.) was used with significance determined at $P < 0.05$.

Results

Screening of oncology drugs to identify agents with ability to induce T-cell chemokine expression

To identify agents capable of enhancing T-cell chemokine expression, we utilized the Approved Oncology Drugs Set consisting of 97 agents. In addition to conventional cytotoxic chemotherapy drugs, this set also includes epigenetic agents and targeted agents such as proteasome and kinase inhibitors. On the basis of the rationale that driver oncogenic mutations may also impact the response to treatment, we used the KRAS-mutant LKR-13 (LKR) lung cancer cell line (16) as a model system as KRAS is frequently mutated in lung adenocarcinoma. The approach to determine concentrations of different agents for equitable comparison was based on their LD_{50} and is described in Supplementary Materials. Expression of T-cell–attracting chemokine genes (*Ccl5*, *Cxcl9*, and *Cxcl10*) is regulated by NF-κB and IFNγ-induced pathways (23, 24); consequently, agents which potentially module activity of these pathways may induce T-cell chemokine expression. Within the subset of agents that induced cytotoxicity (see Supplementary Table S1), several agents (vinrelobine, teniposide, bortezomib, vincristine, romidepsin, vinblastine, and docetaxel) induced *Ccl5* mRNA (>10-fold) in the original screen (Fig. 1A; full list of agents is shown in Supplementary Fig. S1); however, only the HDAC inhibitor (HDACi) romidepsin additionally induced strong expression of *Cxcl9* and *Cxcl10* at LD_{50} concentrations (30 nmol/L; Fig. 1B and C). For *Cxcl10* in particular, this effect of romidepsin was evident across a range of different concentrations (5–30 nmol/L; Supplementary Fig. S2A). An additional HDACi in the Oncology Drugs Set, vorinostat, on the other hand increased *Cxcl9* and *Cxcl10* expression more strongly than *Ccl5* expression (Supplementary Fig. S2B). Focusing on romidepsin, we further confirmed that romidepsin treatment also increased CCL5 and CXCL10 secretion in LKR cells by ELISA (Fig. 1D; CXCL9 was not tested). We further validated enhanced gene expression of *Ccl5*, *Cxcl9*, and *Cxcl10* in the mouse lung cancer cell line 344SQ (17), bearing mutations in KRAS and TP53, and the human A549 lung cancer line (Fig. 1E and F). As *Cxcl10* showed the highest fold induction (Fig. 1E and F), we evaluated changes in expression of this T-cell chemokine in further studies. Ability to induce *CXCL10* gene expression was shared at LD_{50} concentration dosing by several other clinically relevant HDACi MS-275, MGCD0103, LBH-589, and vorinostat in A549 cells (Fig. 1G), and with matching increases in CXCL10 protein levels demonstrated for both romidepsin and vorinostat (Fig. 1H). As myeloid cells are known to express *Ccl5*, *Cxcl9*, and *Cxcl10*, we also tested romidepsin ability to induce these chemokines in Raw 264.7 macrophages. Importantly, romidepsin potently induced gene expression of all 3 chemokines (Fig. 1I). Finally, romidepsin also triggered *Cxcl9* and *Cxcl10* expression in macrophages isolated from LKR tumors (Fig. 1J). These results indicate that among oncology agents in clinical use, HDACi are powerful activators of T-cell chemokine expression.

Antitumor effect of romidepsin accompanies increased T-cell chemokine expression and is critically dependent on T cells

To determine the effects of romidepsin on tumor growth *in vivo*, we implanted LKR cells subcutaneously in syngeneic immunocompetent 129S4/SvJaeJ mice and allowed tumors to grow beyond 200 mm^3 (day 12–14). Romidepsin given on days 14, 16, and 18 after tumor cell inoculation at 2 mg/kg, a dose well below the MTD of 5.6 mg/kg (25), induced a highly significant decrease in tumor growth in LKR ($P = 0.0024$; final tumor volume) (Fig. 2A). While tumor rejection was not observed with this treatment regimen, a prolonged period of stable disease was seen (Fig. 2A). Consistent with *in vitro* studies, we found that whole tumor gene expression of T-cell chemokines was significantly enhanced after romidepsin treatment (Fig. 2B). To determine whether T cells were necessary for the observed response to romidepsin, mice were pretreated with depleting mAbs against both CD4 and CD8 (Supplementary Figs. S3 and S4). Although T-cell depletion did not significantly impact the growth of LKR tumors alone, it completely reversed the antitumor effects of romidepsin ($P < 0.0001$; final tumor volume; Fig. 2C). Thus, a critical mechanism of action of this HDACi likely involves enhancement of antitumor T-cell responses. Furthermore, despite ability to induce cell death *in vitro*, these results indicate that romidepsin does not have a direct therapeutic effect on tumor cells.

Importantly, we observed increase in T-cell infiltration in pooled sets of day 17 LKR tumors after romidepsin treatment, for example, CD4: 0.6% to 1.4% and CD8: 0.9 to 2.7% in the experiment shown (Fig. 2D). However, combined results from three independent experiments showed that a significant increase in infiltration was evident in CD8 but not in CD4 T cells (Fig. 2E). Microarray studies showed that *Ccl5* and *Cxcl9/10* were the only T-cell chemokines induced after romidepsin treatment (Supplementary Table S2). To examine whether T-cell recruitment was necessary for the antitumor effect of romidepsin, we pretreated mice with TAK-779, an inhibitor of CCR5 and CXCR3 (26), the receptors of CCL5 and CXCL9/10/11, respectively. TAK-779 prevented the romidepsin-induced increase in T-cell density (CD4: 1.4% to 0.9% and CD8: 2.7% to 1.2%), but did not reduce steady-state T-cell numbers (CD4: 0.6% to 0.8% and CD8: 0.9 to 1.0%; Fig. 2D). As with a significant increase in CD8 T-cell infiltration after romidepsin treatment, a significant decrease in infiltration after TAK-779 was evident for CD8 but not CD4 T cells in combined results from three independent experiments (Fig. 2E). Although TAK-779 did slightly reduce LKR tumor growth when used alone, it also abrogated the effect of romidepsin treatment, indicating a crucial role for the CCR5 and/or CXCR3 receptors and their respective chemokines (Fig. 2F). Collectively, these findings suggest a mechanism whereby T-cell chemokine expression induced by romidepsin promotes T-cell recruitment, which in turn drives an antitumor response and promotes disease stabilization.

Romidepsin enhances response to anti-PD-1 immunotherapy leading to tumor rejection

The response to PD-1 blockade has been associated with interrelated parameters of T-cell infiltration, an Th1/IFNγ signature, and tumor PD-L1 expression (4, 27–29), suggesting therapies that augment T-cell infiltration or effector function could synergize with checkpoint blockade. We first assessed PD-L1 levels in mouse LKR, 393P, and 344SQ lung cells (16, 17) *in vitro* with or

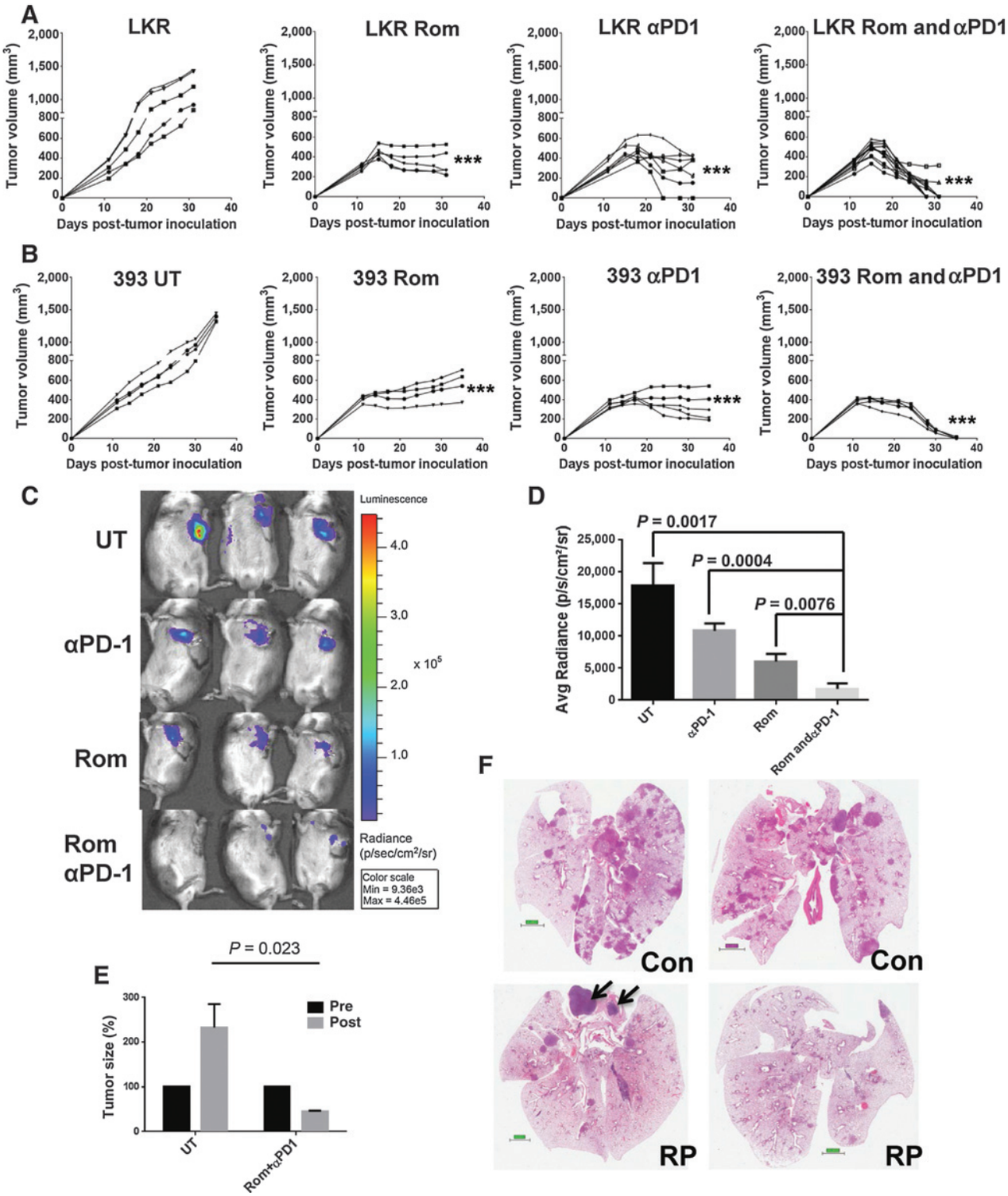

Figure 3.

Romidepsin enhances response to anti-PD-1 immunotherapy leading to tumor rejection. **A,** 129 mice were inoculated and treated with romidepsin (Rom) as in "Fig. 2A" with or without 300 μg/mouse anti-PD-1 antibody on days 15, 17, and 19 as indicated. Significance of tumor size difference is indicated compared with untreated control mice at the last timepoint. **B,** same as in A except 393P (393) tumors were studied. **C,** 50,000 LKR cells were injected in mouse thorax. Treatment regimen was as in "**A**" except it was started on day 6. BLI was performed 14 days after tumor cell injection. **D,** signal of 3 mice/group is shown as mean ± SEM with significance of differences in groups indicated by *P* values. **E,** effect of combined romidepsin and anti-PD-1 treatment in a conditional mutant $KRAS^{G12D}$ autochthonous model of lung cancer. MRI was used to determine total baseline tumor volume (Pre), followed by the initiation of romidepsin and anti-PD-1 treatment (Post). Change in tumor volume (baseline set at 100%) after treatment ($n = 3$) or no treatment (UT, $n = 3$) is indicated over a 1-month period. **F,** H&E staining of two untreated and treated lung specimens from "E". Scale bar = 2 mm. Arrows indicate contaminating lymphoid tissue. RP: Romidepsin and anti-PD-1. Statistical significance is indicated by *P* values or as *, $P < 0.05$; **, $P < 0.01$; ***, $P < 0.001$. NS, not significant.

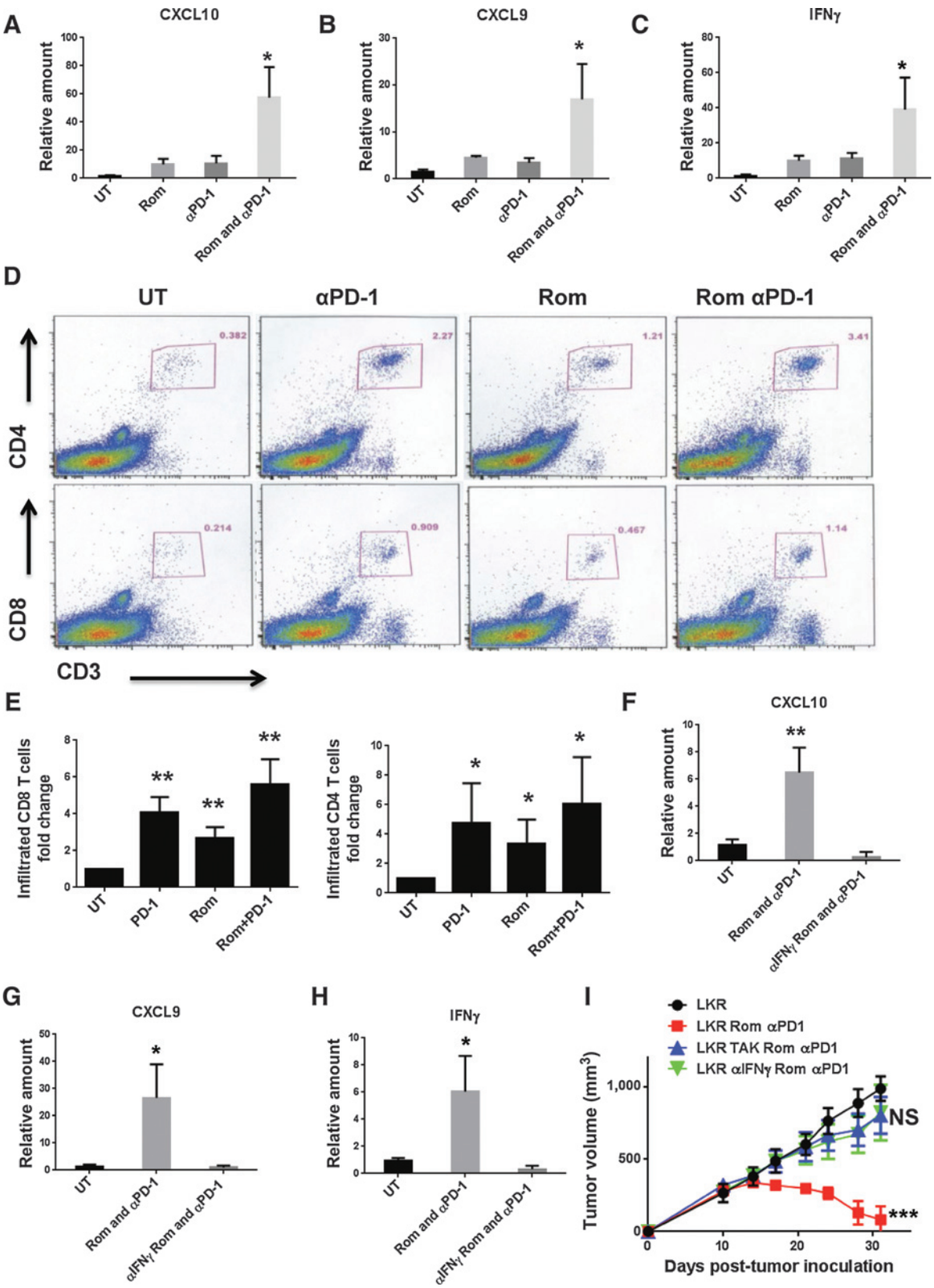

Figure 4.
Crucial requirement for IFNγ in romidepsin and anti-PD-1–induced tumor rejection. **A–C,** *Cxcl10, Cxcl9*, and *Ifng* mRNA expression was determined in subcutaneous LKR tumors by RT-PCR after two romidepsin (Rom) and/or anti-PD-1 antibody injections. Results shown represent 3–4 tumors that were individually analyzed. Significance is indicated compared with untreated control mice. (*Continued on the following page.*)

without 24 hours of exposure to romidepsin or IFNγ. Importantly, romidepsin treatment increased PD-L1 levels although this did not compare in magnitude to the increase observed with IFNγ (Supplementary Fig. S5). We next determined whether LKR tumors were responsive to anti-PD-1 therapy by injecting anti-PD-1 on days 15, 17, and 19 after tumor inoculation. Tumor growth was significantly reduced by anti-PD-1 treatment, but complete rejection was seldom observed over the 30-day period (1/7 mice; Fig. 3A). While occasional tumor rejection was seen over approximately 30 days, longer term follow-up of 47 days in separate experiments showed that neither romidepsin nor anti-PD-1 caused tumor rejection beyond 30 days (Supplementary Fig. S6A). Instead, for both romidepsin and anti-PD-1 treatments, robust tumor growth resumed after a period of stasis (Supplementary Fig. S6A). To evaluate synergism between romidepsin and anti-PD-1 therapy, romidepsin was administered on days 14, 16, and 18, with anti-PD-1 administered on each subsequent day. Combined anti-PD-1 and romidepsin significantly reduced tumor growth compared with individual treatments with romidepsin ($P = 0.0008$) or anti-PD-1 ($P = 0.0041$; Fig. 3A) and rejection was noted in 9 of 11 tumors (Fisher exact test, $P < 0.0001$; Supplementary Fig. S6B). Furthermore, no regrowth of rejected tumors was observed in anti-PD-1 and romidepsin-treated mice (Supplementary Fig. S6C). We also evaluated combination therapy with romidepsin and anti-PD-1 in the 344SQ and 393P tumor models. Tumor rejection was not seen with 344SQ tumors, but combined anti-PD-1 and romidepsin treatment significantly delayed tumor growth compared with either individual treatment (Supplementary Fig. S7). A more pronounced response was observed with 393P tumors, as complete tumor rejections were observed with combination therapy in five of five animals, but in none of the tumor-bearing animals treated with individual agents (Fig. 3B). The striking difference in response in 344SQ and 393P tumor models is, however, not due to differences in oncogene/tumor suppressor mutations as they both harbor KRAS and TP53 mutations (17).

Luciferase-expressing LKR cells were also injected in the lung as an orthotopic tumor model. As with subcutaneous tumors, the greatest antiresponse was seen after combined anti-PD-1 and romidepsin treatment as determined by bioluminescence imaging (BLI; Fig. 3C and D). Finally, we evaluated the effect of combined romidepsin and anti-PD-1 treatment in a conditional mutant $KRAS^{G12D}$ autochthonous knock-in mouse model of lung cancer (20). Tumor growth was initiated by intratracheal injection of replication-deficient adenovirus-expressing CRE recombinase, as described previously (20). Three months later, MRI was used to determine total baseline tumor volume, followed by two rounds of treatment with three doses each of romidepsin and anti-PD-1 treatment. Tumor volume evaluated 1 month after the first MRI increased more than twofold in untreated mice (Fig. 3E). In mice treated with romidepsin and anti-PD-1, tumor volume was significantly reduced by approximately 50% (Fig. 3E). As expected, H&E staining of untreated lung specimens showed significantly larger tumor burden than the lungs of treated mice (Fig. 3F). Together, these findings provide strong rationale for evaluating combined romidepsin and anti-PD-1 mAb therapy in the clinic.

Romidepsin synergizes with IFNγ to enhance tumor immunogenicity

Microarray studies showed that many of the romidepsin-induced genes were known targets of IFNγ (e.g., T-cell chemokines, MHC, and FAS; Supplementary Table S2). Interestingly, expression of the key IFNγ-induced transcription factor STAT1 was also increased by romidepsin (Supplementary Table S2), potentially linking effects of this HDACi to IFNγ signaling. Using additional microarray studies, we tested the possibility that romidepsin may impact IFNγ-induced gene expression. Interestingly, we found that expression of *Ccl5* and *Cxcl9/10* was synergistically increased after romidepsin and IFNγ treatment (Supplementary Fig. S8A). In addition, as with romidepsin alone treatment (Supplementary Table S2), we also found increase in expression of *Stat1* (3 of 45 upregulated probe sets). Interestingly, MHC (*H2k*) and *Fas* gene expression was increased after romidepsin treatment (Supplementary Table S2) but which was not further enhanced by IFNγ. These results indicate that combined romidepsin and IFNγ treatment can potentiate expression of a subset of genes regulated by these agents, including T-cell chemokines and *Stat1*. We validated our microarray data demonstrating increased expression of *Cxcl10* in LKR cells by real-time PCR (Supplementary Fig. S8B). Synergism between romidepsin and IFNγ was also pronounced in 393P cells (Supplementary Fig. S8C).

Previous studies have demonstrated that anti-PD-1 enhances T-cell chemokine expression and T-cell infiltration, and that this effect is mediated by IFNγ production (30). Based upon the ability of IFNγ to synergistically promote chemokine expression with romidepsin *in vitro*, we postulated that IFNγ was also a central regulator of the antitumor response seen with romidepsin and anti-PD-1 *in vivo*. Consistent with this interpretation, combination therapy in mice bearing LKR tumors increased tumor expression of *Cxcl10* and *Cxcl9* by 50-fold and 15-fold, respectively (Fig. 4A and B). This compared to only a 10-fold increase in tumor expression of *Cxcl10* and a fivefold increase in *Cxcl9* in the single-agent control groups (Fig. 4A and B). The chemokine expression pattern was closely matched by increased expression of *Ifng* within the tumors of mice treated with both therapeutic agents (Fig. 4C). Chemokine expression levels correlated with T-cell density, with the highest numbers of CD4 and CD8 T cells present within the tumors of animals treated with combination therapy (Fig. 4D and E).

Crucial requirement for IFNγ in romidepsin and anti-PD-1– induced tumor rejection

We next determined whether IFNγ was functionally required to promote chemokine expression and mediate the antitumor effects

(*Continued.*) **D,** 129 mice with day 14 tumors were untreated (UT) or treated with romidepsin on days 14 and 16 and/or anti-PD-1 antibody on days 15 and 17 after which different group tumors were pooled before FACS to determine CD4 ($CD3^+CD4^+$) and CD8 ($CD3^+CD8^+$) percentages in total viable cells (day 19). **E,** combined results of three independent experiments showing fold increase in presence of CD8 and CD4 T cells in tumors compared with untreated tumors (set at 1) after indicated treatments. Statistical significance (*t* test) is shown for indicated comparisons. **F–H,** same as **A–C** except anti-IFNγ antibody (200 μg/mouse) was injected 2 days prior to the first treatment. **I,** tumor growth showing the effect of TAK-779 (150 μg/mouse) and IFNγ antibody on tumor-bearing mice treated with romidepsin and anti-PD-1 antibody. TAK-779 or IFNγ antibody was injected 2 days prior to romidepsin treatment and continued for twice a week for the length of the experiment. Measurement of five tumors/group are indicated as mean ± SEM. Significance of tumor size difference is indicated compared with untreated control mice at the last timepoint. "ns" indicates not significant.

of combination therapy. To this end, we used an anti-IFNγ antibody to neutralize endogenous IFNγ starting 2 days before initiation of romidepsin/anti-PD-1 treatment. IFNγ neutralization completely abrogated the induction of *Cxcl9*/*Cxcl10* expression within tumors after romidepsin and anti-PD-1 treatment (Fig. 4F and G). Furthermore, neutralization of IFNγ also substantially reduced T-cell infiltration (Supplementary Fig. S9). IFNγ neutralization also blocked the induction of IFNγ gene expression (Fig. 4H), consistent with a feed-forward signaling pathway where production of IFNγ by T cells enhances tumor cell immunogenicity (31), in turn further enhancing T-cell recruitment and function. Finally, we found that IFNγ neutralization ablated the effects of combination therapy, with tumor growth comparable with untreated controls (Fig. 4I). As with reversion of romidepsin therapy alone (Fig. 2F), administration of the CCR5/CXCR3 inhibitor TAK-779 also prevented a response to combination therapy (Fig. 4I). Thus, romidepsin and anti-PD-1 treatments synergize by promoting a chemokine-IFNγ–positive feedback loop through tumor cell and T-cell intermediaries.

Romidepsin synergizes with anti-PD-1 to enhance function of tumor-infiltrating T cells

We next sought to determine potential direct effect of romidepsin on T cells *in vitro* and *in vivo*. First, in T cells stimulated with TCR/CD28 engagement, we did not see any significant impact of romidepsin on IFNγ secretion (Fig. 5A). Previous studies suggest that T cells can also express CCL5 and CXCL10 (32, 33). We therefore next tested the interesting possibility that romidepsin may also induce expression of these chemokines in T cells. Indeed, a substantial increase in expression of *Ccl5* and *Cxcl10* was seen after romidepsin treatment of both CD4 and CD8 T cells (Fig. 5B–D). Therefore, in addition to tumor cells and macrophages, romidepsin can also enhance expression of chemokines in T cells. Finally, we determined whether romidepsin also enhances T-cell functionality *in vivo*. Importantly, the frequency of tumor CD8 and CD4 cells that produce IFNγ *ex vivo* in response to LKR cells in an ELISPOT assay was significantly increased by combination therapy (Fig. 5E and F). This measure of T-cell functionality was not increased by either romidepsin or anti-PD-1 therapy alone, again highlighting the synergistic nature of the combination. Therefore, in addition to promoting T-cell infiltration, romidepsin can also enhance recruited T-cell function in manner that synergizes with PD-1 blockade.

Discussion

Recent clinical studies have demonstrated the considerable potential of immunotherapy in cancer treatment. However, even with combinatorial approaches with anti-CTLA-4 and anti-PD-1, there remain a significant percentage of patients that do not derive a clinical benefit (34). We hypothesized that oncology agents that enhance T-cell recruitment would increase response to immunotherapy. We screened a library of FDA-approved oncology drugs to determine ability to induce expression of *Ccl5*, *Cxcl9*, and *Cxcl10* and found that only a single-agent class, HDACi, was capable of inducing expression of these chemokines. Most importantly, the HDACi romidepsin induced a strong T-cell–dependent antitumor response and combinatory treatment with anti-PD-1–induced tumor regression or rejection across multiple lung tumor models. As multiple HDACi and PD-1 blockade agents (pembrolizumab and nivolumab) are now FDA-approved, combinatory therapy with these two agent classes may represent a promising approach for lung cancer treatment in the near term.

As suggested by recent clinical results (27), the response to anti-PD-1 is restricted by poor T-cell infiltration into tumors. We found that HDACi therapy alone increases tumor expression of *Cxcl9* and *Cxcl10*, promoting T-cell recruitment and a period of tumor stasis (see Fig. 6). The increase in T-cell recruitment was typically more significant for CD8 T cells, the subset strongly implicated in benefit from PD-1 blockade therapy (27). Chemokine expression may depend on multiple cell types as our results indicate romidepsin ability to induce expression in tumor cells, macrophages, and T cells. However, HDACi treatment also upregulated PD-L1 expression, which may limit T -cell functionality (Fig. 6) (35). On the other hand, combination therapy unleashes an IFNγ-dependent response to promote maximal T-cell chemokine expression and T-cell recruitment without sensitization of T cells to the upregulation of PD-L1 on tumor cells (Fig. 6). Limiting CCR5/CXCR3-dependent recruitment of T cells or neutralizing IFNγ prevents response to combination therapy, implicating both steps as critical for therapeutic efficacy. We utilized multiple tumor models (LKR, 393P, and 344SQ) to show greater efficacy of combined treatment versus individual treatments. In the KRAS autochthonous model, however, only the effect of combined romidepsin and anti-PD-1 treatment was studied. Additional studies will therefore be required to determine whether combined treatment is also more efficacious in this model compared with single treatments. Interestingly, recent studies showed reduced immune surveillance in lung adenocarcinoma with mutations in the STK11/LKB1 tumor suppressor (36, 37). The impact of therapeutic regimens identified here on treatment response of KRAS/STK11 as well as the widely used KRAS/TP53 autochthonous model (38) will therefore also be important to determine.

Interestingly, we found that individual depletion of CD4 or CD8 T cells was sufficient to reverse the antitumor effect of romidepsin (Supplementary Fig. S10). In addition to increasing infiltration, an important finding was the increase in tumor-infiltrating CD4 and CD8 function after combination therapy (Fig. 5E and F). This increase may be a consequence of romidepsin-induced increase in tumor cell immunogenicity (e.g., through upregulation of MHC expression), coupled with direct augmentation of T-cell function by anti-PD-1 and potentially by romidepsin (Fig. 6). Interestingly, previous studies indicate that in addition to promoting T-cell recruitment, *Cxcl10* also enhances effector T-cell function (33, 39). Therefore, another interesting possibility is that romidepsin-triggered *Cxcl10* expression synergizes with anti-PD-1 to enhance T-cell function. Further studies will be required to determine specifically how HDACi ± anti-PD-1 modulate T-cell function. An important related issue is the effect of *in vivo* HDAC dose. While we used a dose below the MTD of romidepsin, it is possible that higher dosing may adversely impact function of T cells or other cell types crucial for the antitumor response and thereby reduce therapeutic efficacy. The HDACi dose capable of inducing beneficial epigenetic changes and gene expression but without cytotoxicity towards T cells will also be important to determine for clinical use of these agents when combined with immunotherapeutics. HDACi treatment has previously been reported to induce systemic myeloid-derived suppressor cells

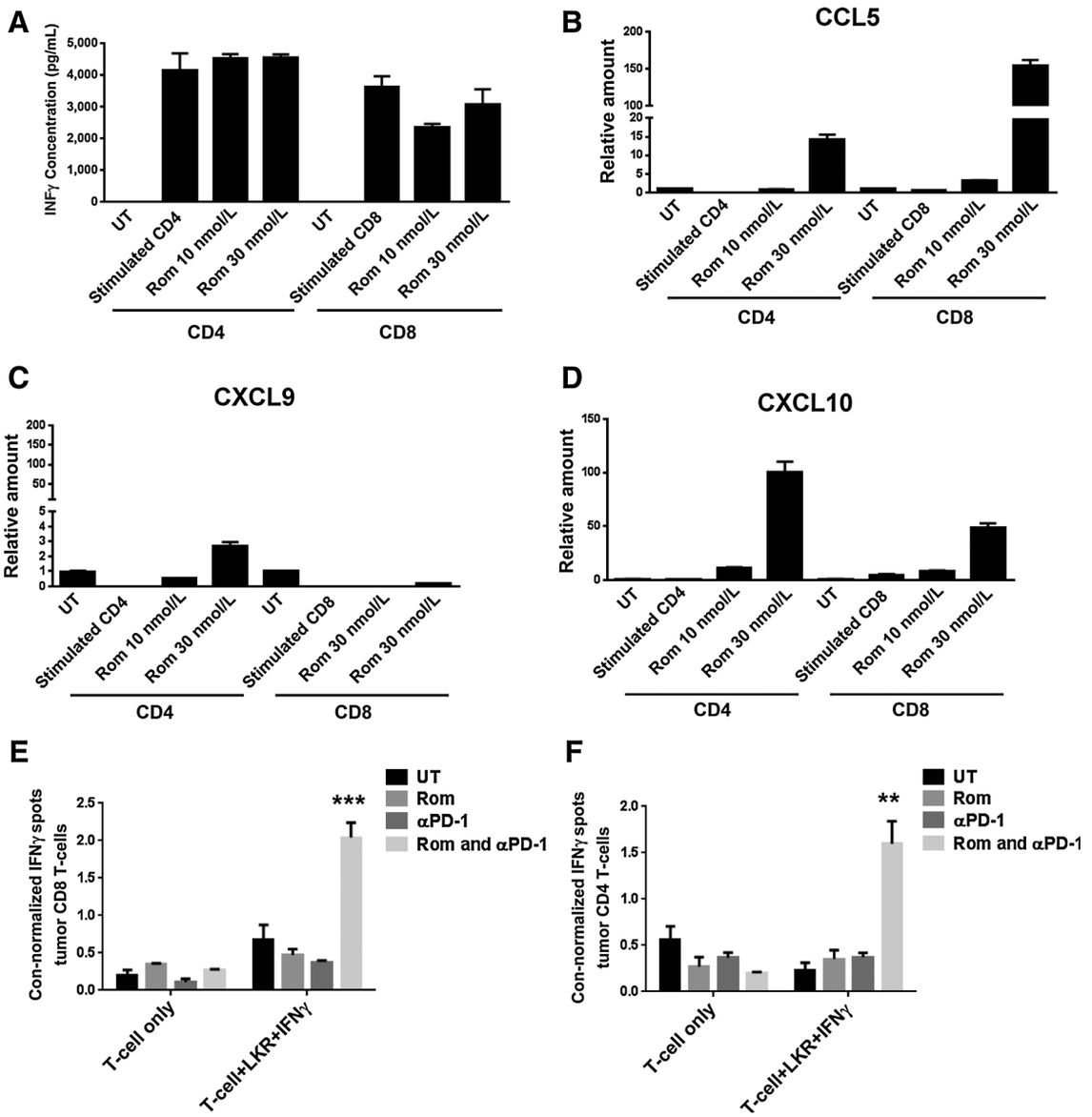

Figure 5.

Romidepsin synergizes with anti-PD-1 to enhance function of tumor-infiltrating T cells. **A,** purified CD4 and CD8 T cells were stimulated with anti-CD3/CD28 (2 μg/mL) for 48 hours followed by addition of romidepsin at indicated concentrations for another 24 hours. Cell culture supernatants were tested for presence of IFNγ using a CBA assay. **B–D,** purified CD4 and CD8 T cells were stimulated as in "**A**" following which mRNA expression of *Ccl5, Cxcl9*, and *Cxcl10* was determined. **E** and **F,** IFNγ ELISPOT of tumor CD8 and CD4 T cells cultured alone, with Concavalin A (ConA) treatment, or with LKR as indicated. T cells, per group, were pooled and samples were run in triplicate (mean ± SEM). Results were normalized to Concavalin A treatment in the same sample T cells. Significance is indicated for comparison of romidepsin+anti-PD-1 treated versus untreated control mice. Rom, romidepsin.

(MDSC) depletion leading enhancement of T-cell responses induced by checkpoint blockade (40). However, we found that romidepsin treatment of mice did not impact MDSC numbers (Supplementary Fig. S11), suggesting that effects of HDACi treatment observed here are not due to MDSC depletion.

Histone modification by histone acetyltransferases (HAT) is typically associated with increased gene expression while removal of acetyl groups by HDACs represses gene expression. Although overall NF-κB activity was crucial for romidepsin-induced T-cell chemokine expression, romidepsin did not enhance nuclear translocation of NF-κB (data not shown). In contrast, romidepsin increased *Stat1* mRNA and further enhanced *Stat1* protein levels after IFNγ treatment (Supplementary Fig. S12). A likely mechanism of synergy may therefore involve IFNγ activation of STAT1 coupled with romidepsin-induced histone modifications to maximize gene expression. It is also likely that genes uniquely regulated by romidepsin or IFNγ act in concert to promote antitumor responses. Interestingly, it was recently shown that romidepsin decreased levels of β-catenin by upregulating expression of its inhibitor SFRP1 (41). In addition, β-catenin signaling was

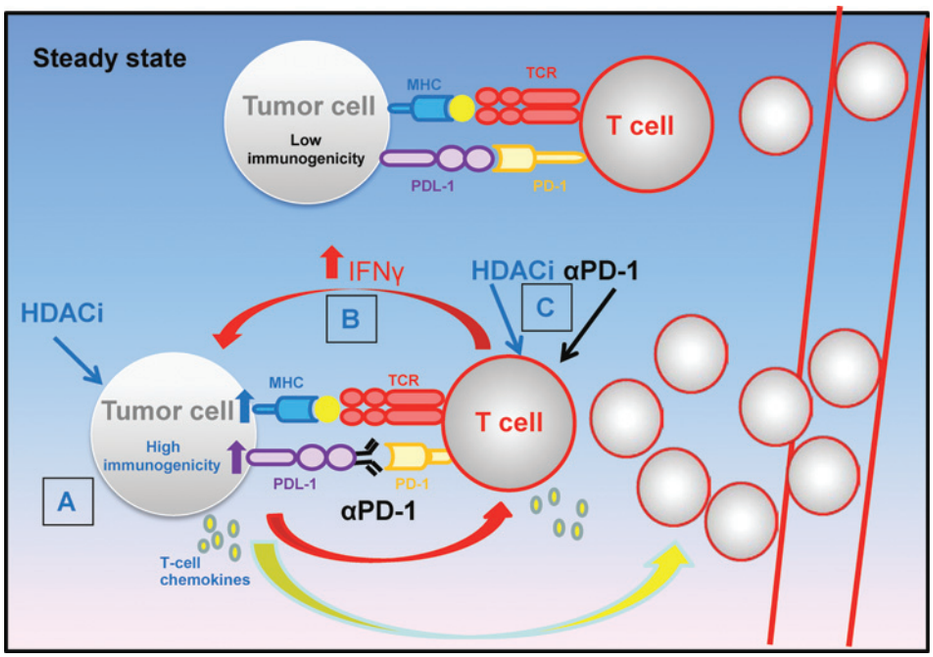

Figure 6.
Model of mechanism of synergy between HDACi and anti-PD-1 treatment. In the steady state, T-cell function is curtailed through multiple immunosuppressive mechanisms including PD-1. In addition, tumor cells have low immunogenicity, including minimal MHC and T-cell chemokine expression, or T-cell infiltration. In the illustrated treatment scenario with HDACi and anti-PD-1, multiple mechanisms are unleashed that contribute towards tumor eradication. **A,** HDACi induce T-cell chemokine expression in multiple cell types, including tumor cells and T cells, resulting in enhanced T-cell recruitment. **B,** when treated with PD-1 blockade and HDACi, anti-PD-1 enhances IFNγ expression in T cells and tumor cells become more responsive to IFNγ through HDACi-mediated effects. This results in high MHC expression and the highest T-cell chemokine expression, which serves to recruit additional T cells. **C,** finally, both anti-PD-1 and HDACi may directly and synergistically enhance T-cell function.

recently shown to suppress checkpoint immunotherapy response (42). An interesting possibility that requires careful examination is whether suppression of β-catenin signaling is an additional mechanism by which romidepsin promotes the anti-PD-1 response.

While the current study focused on pan-HDACi, we also tested HDACi specific for HDAC1+2, HDAC3, HDAC4, HDAC6, and HDAC8. However, we did not observe induction of *Cxcl9*/*10* T-cell chemokine expression as was evident after romidepsin or vorinostat treatment. Additional studies will be required to determine whether these genes are specifically regulated by an HDAC other than the above or whether inhibition of multiple HDACs is required for induction of expression. In an important recent study, it was shown that enhancer of zeste homologue 2 (EZH2)-mediated histone H3 trimethylation (H3K27me3) and DNA methyltransferase 1 (DNMT1)-mediated DNA methylation repress ovarian tumor cell expression of *Cxcl9* and *Cxcl10* (43). Importantly, inhibitors of EZH2, such as DZNep or GSK126, and DNMT1 inhibitor 5-AZA-dC enhance chemokine expression to promote effector T-cell trafficking to the tumor and the response to PD-L1 blockade immunotherapy (43). This study, together with our findings, indicate that regulation of chemokine expression is subject to control by multiple and distinct epigenetic mechanisms. Modulation of tumor immunogenicity by drugs that target epigenetic mechanisms may therefore represent a promising area for translational research and clinical intervention (44).

HDACi are approved for treatment of certain hematologic malignancies, but have failed to demonstrate efficacy in solid tumors. Interestingly, the combination of the HDACi entinostat with 5-AZA-dC has shown benefit in lung cancer treatment, highlighting the potential for HDACi to augment response to other epigenetic therapies (45). Importantly, supportive of our findings, a recent study showed that the HDACi vorinostat increased CD8 T-cell infiltration in human lung tumors (46). In the preclinical setting, there is also evidence of immune modulation by HDACi (47–50). On the basis of the novel findings reported here, we strongly believe that the combination of HDACi with immunotherapy represents a powerful approach for cancer treatment. Notably, several clinical trials employing this combinatory approach are now underway, including one at our institution in patients with NSCLC.

Disclosure of Potential Conflicts of Interest

No potential conflicts of interest were disclosed.

Authors' Contributions

Conception and design: H. Zheng, X. Ren, S.J. Antonia, A.A. Beg
Development of methodology: H. Zheng, W. Zhao, C. Yan, M. Xie, G.V. Martinez, A.A. Beg
Acquisition of data (provided animals, acquired and managed patients, provided facilities, etc.): H. Zheng, C. Yan, C.C. Watson, M. Messengill, C. Messengill, D. Noyes, G.V. Martinez, R. Afzal
Analysis and interpretation of data (e.g., statistical analysis, biostatistics, computational analysis): H. Zheng, C. Yan, M. Messengill, M. Xie, C. Messengill, G.V. Martinez, R. Afzal, Z. Chen, S.J. Antonia, E.B. Haura, A.A. Beg
Writing, review, and/or revision of the manuscript: H. Zheng, C.C. Watson, M. Messengill, C. Messengill, G.V. Martinez, S.J. Antonia, E.B. Haura, B. Ruffell, A.A. Beg

Administrative, technical, or material support (i.e., reporting or organizing data, constructing databases): H. Zheng, M. Xie, R. Afzal, X. Ren, E.B. Haura
Study supervision: H. Zheng, X. Ren, A.A. Beg

Acknowledgments

The authors thank Dr. Kenyon Daniel and Nan Sun (Chemical Biology core) for help setting up chemotherapy agent screening and Dr. Lu Chen for help with statistical analysis, and Dr. J. Kurie (M.D. Anderson Cancer Center, Houston, TX) for providing 393P and 344SQ cells. The authors also acknowledge the help provided by Flow Cytometry, Molecular Genomics, Pathology and Comparative Medicine core facilities at the Moffitt Cancer Center.

Grant Support

This work was supported by lung cancer SPORE P50 CA119997, funds from the Moffitt Cancer Center Lung Cancer Center of Excellence, National Natural Science Foundation of China (grant no. 81472183), and NIH R01 AI0802685.

The costs of publication of this article were defrayed in part by the payment of page charges. This article must therefore be hereby marked *advertisement* in accordance with 18 U.S.C. Section 1734 solely to indicate this fact.

Received October 26, 2015; revised February 16, 2016; accepted March 6, 2016; published OnlineFirst March 10, 2016.

References

1. Pardoll DM. The blockade of immune checkpoints in cancer immunotherapy. Nat Rev Cancer 2012;12:252–64.
2. Sharma P, Allison JP. Immune checkpoint targeting in cancer therapy: toward combination strategies with curative potential. Cell 2015;161:205–14.
3. Brahmer JR, Tykodi SS, Chow LQ, Hwu WJ, Topalian SL, Hwu P, et al. Safety and activity of anti-PD-L1 antibody in patients with advanced cancer. N Engl J Med 2012;366:2455–65.
4. Topalian SL, Hodi FS, Brahmer JR, Gettinger SN, Smith DC, McDermott DF, et al. Safety, activity, and immune correlates of anti-PD-1 antibody in cancer. N Engl J Med 2012;366:2443–54.
5. Twyman-Saint\sVictor C, Rech AJ, Maity A, Rengan R, Pauken KE, Stelekati E, et al. Radiation and dual checkpoint blockade activate non-redundant immune mechanisms in cancer. Nature 2015;520:373–7.
6. Melero I, Berman DM, Aznar MA, Korman AJ, Perez Gracia JL, Haanen J. Evolving synergistic combinations of targeted immunotherapies to combat cancer. Nat Rev Cancer 2015;15:457–72.
7. Adams JL, Smothers J, Srinivasan R, Hoos A. Big opportunities for small moleculesin immuno-oncology. Nat Rev Drug Discov 2015;14:603–22.
8. Zitvogel L, Galluzzi L, Smyth MJ, Kroemer G. Mechanism of action of conventional and targeted anticancer therapies: reinstating immunosurveillance. Immunity 2013;39:74–88.
9. Ma Y, Adjemian S, Mattarollo SR, Yamazaki T, Aymeric L, Yang H, et al. Anticancer chemotherapy-induced intratumoral recruitment and differentiation of antigen-presenting cells. Immunity 2013;38:729–41.
10. Ramakrishnan R, Assudani D, Nagaraj S, Hunter T, Cho HI, Antonia S, et al. Chemotherapy enhances tumor cell susceptibility to CTL-mediated killing during cancer immunotherapy in mice. J Clin Invest 2010;120:1111–24.
11. Ho PC, Bihuniak JD, Macintyre AN, Staron M, Liu X, Amezquita R, et al. Phosphoenolpyruvate is a metabolic checkpoint of anti-tumor T cell responses. Cell 2015;162:1217–28.
12. Ji RR, Chasalow SD, Wang L, Hamid O, Schmidt H, Cogswell J, et al. An immune-active tumor microenvironment favors clinical response to ipilimumab. Cancer Immunol Immunother 2012;61:1019–31.
13. Hopewell EL, Zhao W, Fulp WJ, Bronk CC, Lopez AS, Massengill M, et al. Lung tumor NF-kappaB signaling promotes T cell-mediated immune surveillance. J Clin Invest 2013;123:2509–22.
14. Zhang L, Conejo-Garcia JR, Katsaros D, Gimotty PA, Massobrio M, Regnani G, et al. Intratumoral T cells, recurrence, and survival in epithelial ovarian cancer. N Engl J Med 2003;348:203–13.
15. Pages F, Berger A, Camus M, Sanchez-Cabo F, Costes A, Molidor R, et al. Effector memory T cells, early metastasis, and survival in colorectal cancer. N Engl J Med 2005;353:2654–66.
16. DuPage M, Cheung AF, Mazumdar C, Winslow MM, Bronson R, Schmidt LM, et al. Endogenous T cell responses to antigens expressed in lung adenocarcinomas delay malignant tumor progression. Cancer Cell 2011;19:72–85.
17. Gibbons DL, Lin W, Creighton CJ, Rizvi ZH, Gregory PA, Goodall GJ, et al. Contextual extracellular cues promote tumor cell EMT and metastasis by regulating miR-200 family expression. Genes Dev 2009;23:2140–51.
18. Wang J, Wang X, Hussain S, Zheng Y, Sanjabi S, Ouaaz F, et al. Distinct roles of different NF-kappa B subunits in regulating inflammatory and T cell stimulatory gene expression in dendritic cells. J Immunol 2007;178:6777–88.
19. Valenzuela JO, Iclozan C, Hossain MS, Prlic M, Hopewell E, Bronk CC, et al. PKCtheta is required for alloreactivity and GVHD but not for immune responses toward leukemia and infection in mice. J Clin Invest 2009;119:3774–86.
20. Jackson EL, Willis N, Mercer K, Bronson RT, Crowley D, Montoya R, et al. Analysis of lung tumor initiation and progression using conditional expression of oncogenic K-ras. Genes Dev 2001;15:3243–8.
21. Assudani D, Cho HI, DeVito N, Bradley N, Celis E. In vivo expansion, persistence, and function of peptide vaccine-induced CD8 T cells occur independently of CD4 T cells. Cancer Res 2008;68:9892–9.
22. Ruffell B, Affara NI, Cottone L, Junankar S, Johansson M, DeNardo DG, et al. Cathepsin C is a tissue-specific regulator of squamous carcinogenesis. Genes Dev 2013;27:2086–98.
23. Casola A, Henderson A, Liu T, Garofalo RP, Brasier AR. Regulation of RANTES promoter activation in alveolar epithelial cells after cytokine stimulation. Am J Physiol Lung Cell Mol Physiol 2002;283:L1280–90.
24. Burke SJ, Goff MR, Lu D, Proud D, Karlstad MD, Collier JJ. Synergistic expression of the CXCL10 gene in response to IL-1beta and IFN-gamma involves NF-kappaB, phosphorylation of STAT1 at Tyr701, and acetylation of histones H3 and H4. J Immunol 2013;191:323–36.
25. Imai T, Adachi S, Nishijo K, Ohgushi M, Okada M, Yasumi T, et al. FR901228 induces tumor regression associated with induction of Fas ligand and activation of Fas signaling in human osteosarcoma cells. Oncogene 2003;22:9231–42.
26. Breser ML, Motrich RD, Sanchez LR, Mackern-Oberti JP, Rivero VE. Expression of CXCR3 on specific T cells is essential for homing to the prostate gland in an experimental model of chronic prostatitis/chronic pelvic pain syndrome. J Immunol 2013;190:3121–33.
27. Tumeh PC, Harview CL, Yearley JH, Shintaku IP, Taylor EJ, Robert L, et al. PD-1 blockade induces responses by inhibiting adaptive immune resistance. Nature 2014;515:568–71.
28. Taube JM, Anders RA, Young GD, Xu H, Sharma R, McMiller TL, et al. Colocalization of inflammatory response with B7-h1 expression in human melanocytic lesions supports an adaptive resistance mechanism of immune escape. Sci Transl Med 2012;4:127ra37.
29. Herbst RS, Soria JC, Kowanetz M, Fine GD, Hamid O, Gordon MS, et al. Predictive correlates of response to the anti-PD-L1 antibody MPDL3280A in cancer patients. Nature 2014;515:563–7.
30. Peng W, Liu C, Xu C, Lou Y, Chen J, Yang Y, et al. PD-1 blockade enhances T-cell migration to tumors by elevating IFN-gamma inducible chemokines. Cancer Res 2012;72:5209–18.
31. Dunn GP, Koebel CM, Schreiber RD. Interferons, immunity and cancer immunoediting. Nat Rev Immunol 2006;6:836–48.
32. Cocchi F, DeVico AL, Garzino-Demo A, Arya SK, Gallo RC, Lusso P. Identification of RANTES, MIP-1 alpha, and MIP-1 beta as the major HIV-suppressive factors produced by CD8+ T cells. Science 1995;270:1811–5.
33. Peperzak V, Veraar EA, Xiao Y, Babala N, Thiadens K, Brugmans M, et al. CD8+ T cells produce the chemokine CXCL10 in response to CD27/CD70 costimulation to promote generation of the CD8+ effector T cell pool. J Immunol 2013;191:3025–36.
34. Larkin J, Chiarion-Sileni V, Gonzalez R, Grob JJ, Cowey CL, Lao CD, et al. Combined nivolumab and ipilimumab or monotherapy in untreated melanoma. N Engl J Med 2015;373:23–34.

35. Woods DM, Sodre AL, Villagra A, Sarnaik A, Sotomayor EM, Weber J. HDAC inhibition upregulates PD-1 ligands in melanoma and augments immunotherapy with PD-1 blockade. Cancer Immunol Res 2015;3: 1375–85.
36. Schabath MB, Welsh EA, Fulp WJ, Chen L, Teer JK, Thompson ZJ, et al. Differential association of STK11 and TP53 with KRAS mutation-associated gene expression, proliferation and immune surveillance in lung adenocarcinoma. Oncogene. 2015 Oct 19. [Epub ahead of print].
37. Skoulidis F, Byers LA, Diao L, Papadimitrakopoulou VA, Tong P, Izzo J, et al. Co-occurring genomic alterations define major subsets of KRAS-mutant lung adenocarcinoma with distinct biology, immune profiles, and therapeutic vulnerabilities. Cancer Discov 2015;5:860–77.
38. Chen Z, Cheng K, Walton Z, Wang Y, Ebi H, Shimamura T, et al. A murine lung cancer co-clinical trial identifies genetic modifiers of therapeutic response. Nature 2012;483:613–7.
39. Dufour JH, Dziejman M, Liu MT, Leung JH, Lane TE, Luster AD. IFN-gamma-inducible protein 10 (IP-10; CXCL10)-deficient mice reveal a role for IP-10 in effector T cell generation and trafficking. J Immunol 2002;168: 3195–204.
40. Kim K, Skora AD, Li Z, Liu Q, Tam AJ, Blosser RL, et al. Eradication of metastatic mouse cancers resistant to immune checkpoint blockade by suppression of myeloid-derived cells. Proc Natl Acad Sci U S A 2014; 111:11774–9.
41. Valdez BC, Brammer JE, Li Y, Murray D, Liu Y, Hosing C, et al. Romidepsin targets multiple survival signaling pathways in malignant T cells. Blood Cancer J 2015;5:e357.
42. Spranger S, Bao R, Gajewski TF. Melanoma-intrinsic beta-catenin signalling prevents anti-tumour immunity. Nature 2015;523:231–5.
43. Peng D, Kryczek I, Nagarsheth N, Zhao L, Wei S, Wang W, et al. Epigenetic silencing of TH1-type chemokines shapes tumour immunity and immunotherapy. Nature 2015;527:249–53.
44. Maio M, Covre A, Fratta E, Di Giacomo AM, Taverna P, Natali PG, et al. Molecular pathways: at the crossroads of cancer epigenetics and immunotherapy. Clin Cancer Res 2015;21:4040–7.
45. Juergens RA, Wrangle J, Vendetti FP, Murphy SC, Zhao M, Coleman B, et al. Combination epigenetic therapy has efficacy in patients with refractory advanced non-small cell lung cancer. Cancer Discov 2011;1: 598–607.
46. Ma T, Galimberti F, Erkmen CP, Memoli V, Chinyengetere F, Sempere L, et al. Comparing histone deacetylase inhibitor responses in genetically engineered mouse lung cancer models and a window of opportunity trial in patients with lung cancer. Mol Cancer Ther 2013;12: 1545–55.
47. Vo DD, Prins RM, Begley JL, Donahue TR, Morris LF, Bruhn KW, et al. Enhanced antitumor activity induced by adoptive T-cell transfer and adjunctive use of the histone deacetylase inhibitor LAQ824. Cancer Res 2009;69:8693–9.
48. Christiansen AJ, West A, Banks KM, Haynes NM, Teng MW, Smyth MJ, et al. Eradication of solid tumors using histone deacetylase inhibitors combined with immune-stimulating antibodies. Proc Natl Acad Sci U S A 2011;108: 4141–6.
49. West AC, Mattarollo SR, Shortt J, Cluse LA, Christiansen AJ, Smyth MJ, et al. An intact immune system is required for the anticancer activities of histone deacetylase inhibitors. Cancer Res 2013;73:7265–76.
50. West AC, Johnstone RW. New and emerging HDAC inhibitors for cancer treatment. J Clin Invest 2014;124:30–9.